

# Small antibody mimetics comprising two complementarity-determining regions and a framework region for tumor targeting

Xiao-Qing Qiu<sup>1</sup>, He Wang<sup>3</sup>, Bei Cai<sup>2</sup>, Lan-Lan Wang<sup>2</sup> & Shi-Tao Yue<sup>1</sup>

Here we show that fusion of two complementarity-determining regions (CDRs), V<sub>H</sub>CDR1 and V<sub>L</sub>CDR3, through a cognate framework region (V<sub>H</sub>FR2) yields mimetics that retain the antigen recognition of their parent molecules, but have a superior capacity to penetrate tumors. The antigen-recognition abilities of these ~3 kDa mimetics surpass those of comparable fragments lacking the framework region. *In vivo* activities of the mimetics suggests that the structural orientation of their CDRs approximates the conformation of the CDRs in the complex of the parent antibody with antigen. We linked the antibody mimetics to the bacterial toxin colicin Ia to create fusion proteins called “pheromonicins,” which enable targeted inhibition of tumor growth. In mice bearing human malignant tumors, pheromonicins directed against tumor-specific surface markers show greater capacity to target and penetrate tumors than their parent antibodies. Rational recombination of selected V<sub>H</sub>/V<sub>L</sub> binding sites and their framework regions might provide useful targeting moieties for cytotoxic cancer therapies.

The limited ability of native antibodies and antibody fragments to penetrate solid cancers has stimulated the search for smaller alternatives. Most approaches have focused on developing antibody fragments derived from the three antigen-binding entities that reside in a variable domain of either the heavy chain (V<sub>H</sub>) or light chain (V<sub>L</sub>) of the antigen-binding fragment (Fab) of immunoglobulins. Although it is accepted that antigen recognition by whole antibodies requires multiple noncovalent forces involving all six CDR loops residing in the V<sub>H</sub> and V<sub>L</sub> domains<sup>1–5</sup>, the contributions of synergic interactions of V<sub>H</sub> and V<sub>L</sub> domains are not well understood<sup>1,4,5–7</sup>. Derivatives of CDR sequences retain antigen-recognition abilities<sup>3,8,9</sup>, but antibody mimetics with modified CDR structure are inactive *in vivo*, possibly owing to inappropriate CDR modification or the absence of spacers between the CDR derivatives<sup>9,10</sup>, which could mimic the four framework regions that separate the hypervariable regions of the variable domains.

We used CDR and framework region sequences from a monoclonal IgG against the Epstein-Barr virus (EBV) envelope antigen gp350/220 to create several single-chain antibody mimetics comprising two interacting V<sub>H</sub>- and V<sub>L</sub>-derived CDRs. Our goals were to establish whether the mimetics retain the antigen-recognition ability of the V<sub>H</sub>/V<sub>L</sub> interaction observed in whole antibodies and whether this might be exploited to create smaller, high-affinity binders of therapeutic value. The framework region from either the V<sub>H</sub> or V<sub>L</sub> domain orients the two CDRs in a manner resembling their disposition in native molecules (Fig. 1a).

Design of the mimetics was guided by four precepts. First, as antigen recognition by intact Fab is synergistically produced by all

six CDRs residing in both the V<sub>H</sub> and V<sub>L</sub> domains, it should contain at least two antigen-binding sites: one from the V<sub>H</sub> and the other from the V<sub>L</sub> domain. Such synergistic recognition cannot be accomplished if the CDR loops all originate from one variable domain<sup>1,3–9,11–14</sup>. Second, as the CDR3 loop is the central, most accessible antigen-binding segment in an intact Fab, it should be regarded as an essential component of the mimetic<sup>2–5,8,12</sup>. Third, the CDR3 loop should be complemented by either the CDR1 or CDR2 loop of the other variable domain, as these are normally the closest to CDR3 in the parental antibody. Fourth, the C-terminus of the selected CDR1 or CDR2 loop and the N-terminus of the selected CDR3 loop should be joined with a framework region selected from either the V<sub>H</sub> or the V<sub>L</sub> to approximate the linkage of CDR in the parent molecule.

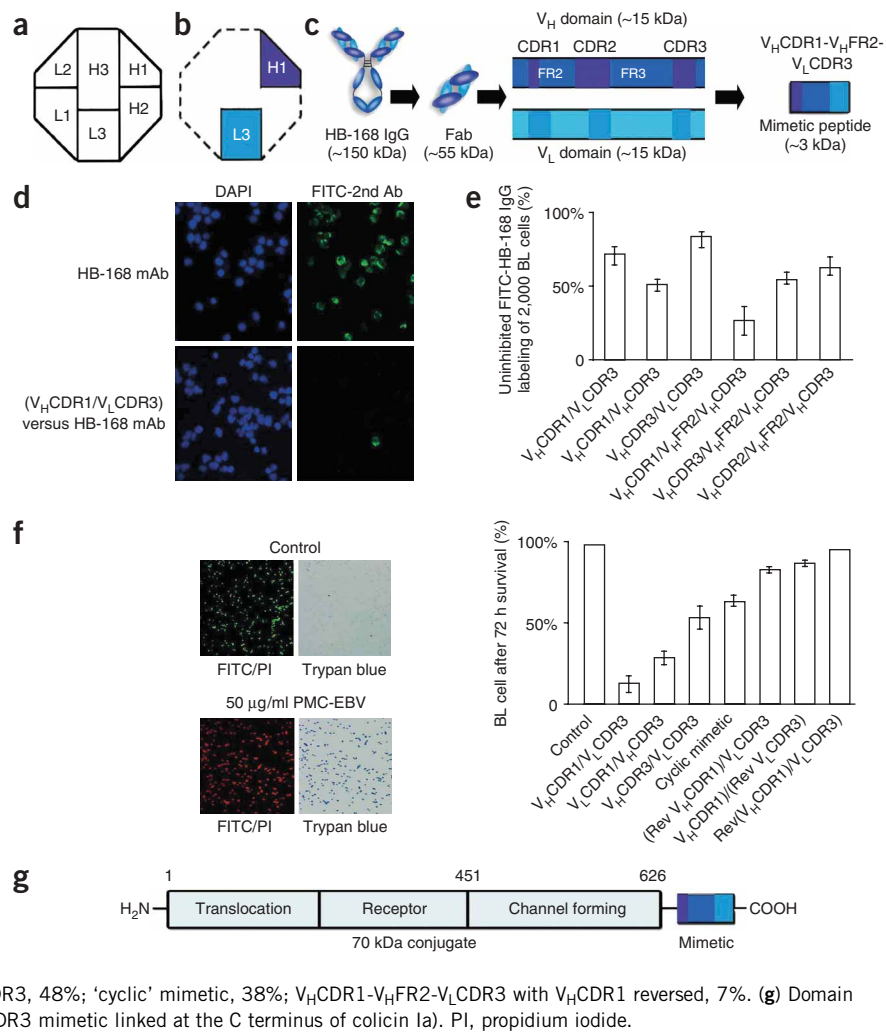
Guided by *in vitro* binding assays of these variants derived from the anti-gp350/220 IgG, which suggested that the V<sub>H</sub>CDR1-V<sub>H</sub>FR2-V<sub>L</sub>CDR3 derivative showed most promise, we designed three other ~3-kDa mimetics that also comprise cognate V<sub>H</sub>CDR1 and V<sub>L</sub>CDR3 connected by the corresponding V<sub>H</sub>FR2 sequence. The parent molecules from which these were derived are a monoclonal IgM against surface antigen of non-small-cell lung cancer cells, a monoclonal IgG against CD8 and a single-chain Fv (scFv) antibody fragment against CD23 lymphocyte differentiation antigens<sup>15–19</sup>.

Structurally, each is neither a derivative of a single-domain antibody in which all components came from one variable domain<sup>1,5,13,14</sup>, nor a microantibody, which is typically defined as a peptide derived from a single CDR<sup>8</sup>. However, like antibodies and antibody fragments, each mimetic can be linked to an indicator (e.g., a cytotoxin) to evaluate its

<sup>1</sup>Key Laboratory of Transplant Immunology, Ministry of Health, State Key Laboratory of Biotherapy, and <sup>2</sup>Department of Lab Medicine, Division of Clinical Immunology, West China Hospital. <sup>3</sup>Laboratory of Genetics, West China Second University Hospital, West China School of Medicine, Sichuan University, No. 37 Wai Nan Guo-xue-Xiang, Chengdu, P.R. of China 610041. Correspondence should be addressed to X.-Q.Q. (xqiu@tfol.com).

Received 2 January; accepted 11 June; published online 5 August 2007; doi:10.1038/nbt1320

**Figure 1** Structure and activity of mimetics and fusion molecules. **(a,b)** In contrast with the antibody-binding-site surface, where the CDR3 regions of  $V_H$  and  $V_L$  domains are surrounded by peripheral CDRs **(a)**, the mimetic-binding-site surface comprises only two CDRs,  $V_H$ CDR1 and  $V_L$ CDR3 **(b)**. **(c)** Structure of a 28-residue mimetic comprising the  $V_H$ CDR1,  $V_H$ FR2 and  $V_L$ CDR3 domains of Fab, compared with IgG and Fab. **(d,e)** Fixed BL cells were incubated with either synthetic mimetics (50  $\mu$ M) or 10 mM PBS, then incubated with HB-168 IgG (5  $\mu$ M), FITC-labeled secondary antibody (5  $\mu$ M) and DAPI (30 ng/ml) prior to cell-counting **(d)** and flow cytometry **(e)** on treated cells. In **d**, FITC-labeled secondary antibodies revealed the binding of HB-168 IgG with EBV antigens at the surface of BL cells. In the presence of synthetic  $V_H$ CDR1- $V_H$ FR2- $V_L$ CDR3 mimetics, 95% of IgG binding was eliminated. **(f)** The cytotoxicity of all fusion peptides with corresponding mimetics of HB-168 IgG was determined by incubating EBV-induced BL cells with the respective fusion peptides (50  $\mu$ g/ml) for 72 h, then staining treated cells with 50 nM acridinorange/600 nM propidium iodide (left panel) and 0.4% Trypan blue (right panel) and collecting five fields of optical/fluorescent images at 160 $\times$  magnification for cell counting. The survival cell ratio of all view fields (about  $2-4 \times 10^3$  cells) was obtained as the following quotient: (sum of living cells)/(sum of living cells + sum of dead cells). Living cell, green or transparent; dead cell, red or dark blue. Histogram shows percentage of surviving BL cells ( $2-4 \times 10^3$  cells counted) after 72 h *in vitro* treatment with fusion peptides (50  $\mu$ g/ml). The killing ability of fusion peptides was obtained as the reciprocal of survival;  $V_H$ CDR1- $V_H$ FR2- $V_L$ CDR3, 88%;  $V_L$ CDR1- $V_L$ FR2- $V_H$ CDR3, 72%;  $V_H$ CDR3- $V_H$ FR2- $V_L$ CDR3, 48%; 'cyclic' mimetic, 38%;  $V_H$ CDR1- $V_H$ FR2- $V_L$ CDR3 with  $V_H$ CDR1 reversed, 7%. **(g)** Domain diagram of the fusion molecule ( $V_H$ CDR1- $V_H$ FR2- $V_L$ CDR3 mimetic linked at the C terminus of colicin Ia).



antigen recognition ability *in vitro* and *in vivo*. Fusion of our antibody mimetics to the C-terminus of colicin Ia, a 70-kDa member of the E1 colicin family of channel-forming bacteriocins that are bactericidal to *Escherichia coli*<sup>20</sup>, enabled us to demonstrate their ability to target and kill cancer cells within solid tumors bearing specific surface antigens. Colicin Ia kills target cells by forming a voltage-activated channel in the target cell membrane, mediated by its 175-residue, C-terminal, channel-forming domain<sup>21-25</sup>.

## RESULTS

### Construction of mimetics and toxin-mimetic fusion peptides

As the CDR3 loops of the  $V_H$  and  $V_L$  domains are the accessible entities that interact with antigenic epitopes<sup>2,5,12,14</sup> (Fig. 1a,b), we defined a CDR3 domain of either the  $V_H$  or  $V_L$  domain of a Fab fragment as the key component of our prototype antibody mimetic. If either the CDR1 or CDR2 loop of the other variable domain is selected as the complementary component, there are four ordered pairs of CDR loops that could be recombined for constructing mimetics. The C terminus of the selected CDR1 or CDR2 loop and the N terminus of the selected CDR3 loop must be linked by the framework region with the fewest hydrophobic patches to approximate the linkage of CDR in the parent Fab. We synthesized four mimetics of HB-168 IgG, a monoclonal IgG against EBV gp350/220 envelope glycoprotein. Two comprised either  $V_H$ CDR1 or  $V_H$ CDR2

linked to  $V_L$ CDR3 by  $V_H$ FR2, whereas the other two comprised either  $V_L$ CDR1 or  $V_L$ CDR2 linked to  $V_H$ CDR3 by  $V_L$ FR2 (Fig. 1c). Of four control mimetics, two were prepared by connecting (i)  $V_H$ CDR3 to  $V_L$ CDR3 and (ii)  $V_H$ CDR1 to  $V_H$ CDR3 via  $V_H$ FR2. Another two mimetics, comprising either  $V_H$ CDR1 linked to  $V_L$ CDR3 or  $V_H$ CDR3 linked to  $V_L$ CDR3, but without a framework region linker were synthesized to determine the contribution of the framework region connection. Previous studies found that mimetics made with reduced/replaced derivations of partial CDRs selected from  $V_H$  and  $V_L$  domains possessed some antigen-recognition activity<sup>10</sup>.

The antigen-recognition capabilities of all mimetics were assessed by competition with the parent antibody against EBV-induced Burkitt's lymphoma (BL) cells. The results (Fig. 1d,e) indicated that (i) the  $V_H$ CDR1- $V_H$ FR2- $V_L$ CDR3 mimetic had the strongest effect on blocking binding of the parent antibody, (ii) mimetics comprised of CDRs and a framework region selected from either  $V_H$  or  $V_L$  possess superior binding abilities to those without the framework region connecting the CDRs and (iii) when connected to the CDR3 loop of the other variable domain, the CDR1 loop confers binding superior to the CDR2 domain.

To create toxin fusions to HB-168 mimetics, we cloned DNA encoding the 3' end of the sequence encoding colicin Ia in frame to the following four fragments: (i)  $V_H$ CDR1- $V_H$ FR2- $V_L$ CDR3, (ii)  $V_L$ CDR1- $V_L$ FR2- $V_H$ CDR3, (iii)  $V_H$ CDR3- $V_H$ FR2- $V_L$ CDR3 and

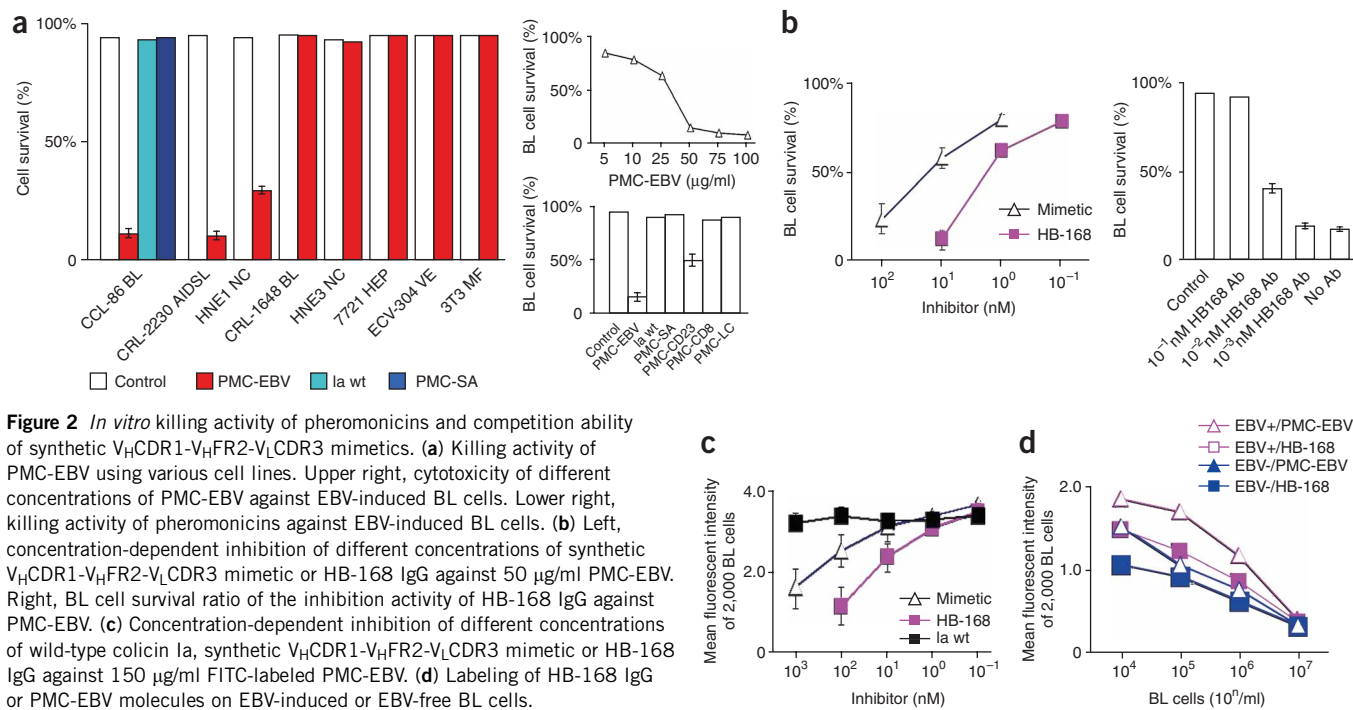


**Figure 2** *In vitro* killing activity of pheromonicins and competition ability of synthetic V<sub>H</sub>CDR1-V<sub>H</sub>FR2-V<sub>L</sub>CDR3 mimetics. (a) Killing activity of PMC-EBV using various cell lines. Upper right, cytotoxicity of different concentrations of PMC-EBV against EBV-induced BL cells. Lower right, killing activity of pheromonicins against EBV-induced BL cells. (b) Left, concentration-dependent inhibition of different concentrations of synthetic V<sub>H</sub>CDR1-V<sub>H</sub>FR2-V<sub>L</sub>CDR3 mimetic or HB-168 IgG against 50 μg/ml PMC-EBV. Right, BL cell survival ratio of the inhibition activity of HB-168 IgG against PMC-EBV. (c) Concentration-dependent inhibition of different concentrations of wild-type colicin Ia, synthetic V<sub>H</sub>CDR1-V<sub>H</sub>FR2-V<sub>L</sub>CDR3 mimetic or HB-168 IgG against 150 μg/ml FITC-labeled PMC-EBV. (d) Labeling of HB-168 IgG or PMC-EBV molecules on EBV-induced or EBV-free BL cells.

(iv) a ‘cyclic’ mimetic containing ‘active’ polar and hydrophobic residues of all six CDRs in an HB-168 IgG Fab, which contains interspersed proline residues for flexibility as well as N-terminal cysteine and C-terminal methionine residues for proposed cyclization<sup>9,24</sup> (Supplementary Fig. 1 online). An *in vitro* cytotoxicity assay involving EBV-induced BL cells indicated that fusion of colicin to the V<sub>H</sub>CDR1-V<sub>H</sub>FR2-V<sub>L</sub>CDR3 mimetic showed the most effective killing activity. Fusions of colicin to scrambled V<sub>H</sub>CDR1-V<sub>H</sub>FR2-V<sub>L</sub>CDR3, in which either the V<sub>H</sub>CDR1 or the V<sub>L</sub>CDR3 alone or the entire V<sub>H</sub>CDR1-V<sub>H</sub>FR2-V<sub>L</sub>CDR3 was scrambled, as well as fusion of colicin to the ‘cyclic’ mimetic, showed ~3–5 times less killing activity than the V<sub>H</sub>CDR1-V<sub>H</sub>FR2-V<sub>L</sub>CDR3 fusion peptide at the same concentration (Fig. 1f).

Based on these results, we used V<sub>H</sub>CDR1-V<sub>H</sub>FR2-V<sub>L</sub>CDR3 mimetics of HB-168 IgG, HB-8627 IgM against non-small-cell lung cancer antigen, IgG against CD8, or scFv against CD23 lymphocyte differentiation antigens for subsequent studies (Supplementary Fig. 1 online). Fusion of these mimetics to the C terminus of colicin Ia created four toxin-mimetic fusion peptides, or pheromonicins, subsequently referred to as pheromonicin-EBV (PMC-EBV), PMC-LC, PMC-CD8 and PMC-CD23 (Fig. 1g). Data from SDS-PAGE and sizing chromatography are consistent with expression of the fusion and the absence of aggregation in labeled PMC-EBV and HB-168 IgG preparations (Supplementary Fig. 2 online). The pheromonicin formed voltage-activated channels in artificial planar lipid bilayer membranes with a gating pattern similar to that of wild-type colicin Ia channels (Supplementary Fig. 2 online)<sup>21,26</sup>.

#### *In vitro* killing activity of V<sub>H</sub>CDR1-V<sub>H</sub>FR2-V<sub>L</sub>CDR3 fusion peptides

EBV-induced BL cells were incubated with various concentrations of different pheromonicins to determine the *in vitro* killing activity (Fig. 2a). Neither wild-type colicin Ia nor PMC-SA, a staphylococcal pheromone-colicin Ia fusion peptide<sup>24</sup>, killed BL cells up to the maximal concentration tested (125 μg/ml) (Fig. 2a). In contrast, at

concentrations ≥ 50 μg/ml, PMC-EBV killed 90% of BL cells (Fig. 2a). PMC-LC and PMC-CD8 had killing activity against corresponding CCL-185 non-small cell lung carcinoma and TIB-152 T-cell leukemia cells, but not against BL cells (Fig. 2a; Supplementary Fig. 3 online). In contrast, PMC-CD23 had killing activity against EBV-induced and EBV-free BL cells because both carried CD23 antigens on their surface (Fig. 2a; Supplementary Fig. 3 online).

PMC-EBV molecules presented dramatic killing effects against EBV-induced BL, AIDS-related, body cavity-based lymphoma and nasopharyngeal cancer cells, as well as PMC-LC against non-small cell lung cancer and PMC-CD8 or PMC-CD23 against corresponding T or B lymphatic tumor cells (Supplementary Fig. 3 online). Of these cells, 50–90% were killed within 72–96 h after exposure to the pheromonicin, recognizing its cognate cell-surface antigen ( $P < 0.001$ ). In contrast, 96 h incubation of human EBV-free BL cells, nasopharyngeal cancer cells, hepatoma cells, venous endothelia and mouse 3T3 fibroblasts in the presence of PMV-EBV (50–125 μg/ml) did not affect viability of these cells relative to untreated controls (Fig. 2a).

#### *In vitro* specificity of V<sub>H</sub>CDR1-V<sub>H</sub>FR2-V<sub>L</sub>CDR3 fusion peptides

Exposure of EBV-free cells to PMC-CD23, but not to PMC-EBV, inhibited cell growth (Supplementary Fig. 3 online). Similarly, neither the fusion peptides with the reversed V<sub>H</sub>CDR1-V<sub>H</sub>FR2-V<sub>L</sub>CDR3 mimetic, nor HB-168 IgG, PMC-LC or PMC-CD8 alone had evident inhibitory effects on growth of EBV-induced BL cells (Figs. 1f and 2a). The killing activity of PMC-EBV molecules against BL cells could be inhibited up to 90% by increasing concentrations of free HB-168 IgG or synthetic V<sub>H</sub>CDR1-V<sub>H</sub>FR2-V<sub>L</sub>CDR3 mimetics molecules (Fig. 2b). When we compared the competitive binding activity of synthetic mimetic and parent antibody molecules against PMC-EBV, flow cytometry indicated that at the range of 1–1 × 10<sup>3</sup> nM inhibitor, binding activity of the synthetic V<sub>H</sub>CDR1-V<sub>H</sub>FR2-V<sub>L</sub>CDR3 mimetic molecules was reduced at least 10- to 100-fold compared with that of the parent antibody (Fig. 2c). In contrast, wild-type colicin Ia had no

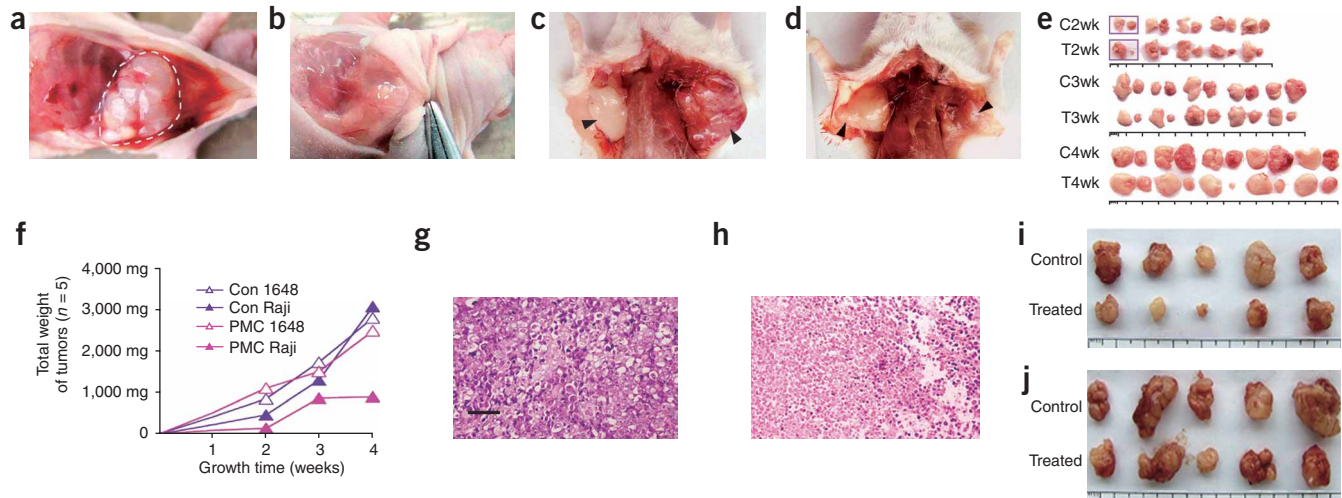


**Figure 3** *In vivo* effects of PMC-EBV against solid tumors. Mice bearing tumors were inoculated with Burkitt's lymphoma (BL) cells or non-small lung cancer or small cell lung cancer cells respectively. Specimens were stained with hematoxylin and eosin. Tumors are marked by dotted lines. (a,b) BALB/c mouse bearing 28-d-old EBV-infected BL tumor either as control (a) or with 20-d PMC-EBV treatment (b). (c,d) SCID mice bearing 31-d-old EBV-free (left side) and EBV-induced tumors (right side) either as control (c) or with 30-d PMC-EBV treatment (d). (e) The tumors of mice (control,  $n = 5$ , treated,  $n = 5$ ) bearing EBV-free (left side) and EBV-induced (right side) tumors were collected 2, 3 or 4 weeks later. C2wk, control; T2wk, treated for 2 weeks; C3wk, control; T3wk, treated for 3 weeks; C4wk, control; T4wk, treated for 4 weeks. Blue rectangles outline the EBV-induced (right) and EBV-free (left) tumors in each mouse. (f) The weights of each individual tumor in e were added together and the sums of weights were compared. Con and PMC 1648, EBV-free tumors of control and treated mice, Con and PMC Raji, EBV-induced tumors of control and treated mice. (g) 400 $\times$  view shows that EBV-infected tumor proliferated in controls. Conversely, extensive coagulated necrosis appeared in the EBV-infected tumor with PMC-EBV treatment (h). (i,j) Non-small cell (i) and small cell (j) lung cancers of each mouse were collected at the end of the 2-week experimental period. Control, untreated cancer; Treated, cancer treated with PMC-LC. Scale bar in g, 50  $\mu$ m.

such binding activity (Fig. 2c). Furthermore, the HB-168 or PMC-EBV labeling on EBV-induced or EBV-free BL cells revealed more details about the variations in affinity of PMC-EBV molecules. At  $10^4$ – $10^6$  cells/ml, the PMC-EBV molecules showed nearly twice the affinity of the parent antibody for EBV-induced BL cells, but about the same affinity as the parent antibody for potential cross-reactive antigen of EBV-free cells (Fig. 2d). These data strongly suggest that the  $V_H$ CDR1- $V_H$ FR2- $V_L$ CDR3 mimetic retained reduced affinity from the parent antibody but the targeting specificity of the fusion peptides absolutely relied on the interaction between the mimetic and related antigenic epitopes on the surface of targeted cells.

#### *In vivo* activity of $V_H$ CDR1- $V_H$ FR2- $V_L$ CDR3 fusion peptides

To assess whether fusion peptides inhibit the proliferation of implanted solid tumors *in vivo*, we established solid tumor models in two strains of immunocompromised mice by inoculating them with EBV-induced or EBV-free human malignant lymphoma, non-small cell lung cancer or small-cell lung cancer ( $0.2$ – $0.3$  ml,  $3$ – $5 \times 10^8$  cells/ml).

BALB/c nude mice were inoculated with EBV-induced BL cells in the left armpit and a 20-d treatment was started 8 d after inoculation. At the end of the experimental period, tumors of control mice ( $n = 10$ , intraperitoneal control solution 0.5 ml/day) were as large as  $8 \times 6 \times 4$  mm (Fig. 3a), whereas all tumors of treated mice ( $n = 10$ , intraperitoneal PMC-EBV 350  $\mu$ g/day) either disappeared or shrank to  $< 1$  mm $^3$ . Autopsy revealed either no visible tumor or tumors smaller than 1 mm $^3$  (Fig. 3b). Microscopic examination revealed that tumor cells underwent extensive coagulative necrosis after treatment, leaving only necrotic entities at the end of the experimental period (Supplementary Fig. 4 online). Comparison of the combined weights of all tumors revealed statistically significant differences in the sums of the tumor weights between control and

treated BL lymphoma ( $P < 0.05$ , rank-order analysis, Mann-Whitney test) (Table 1).

Each severe combined immunodeficient (SCID) mouse was inoculated with EBV-induced BL cells in the left armpit and with EBV-free BL cells in the right armpit (Fig. 3c,d). A 30-d treatment was started 2 d after the inoculation by intraperitoneal injection twice a day. All tested mice were divided into three groups, each containing five control (control solution, 0.5 ml/12 h) and five treated (PMC-EBV, 350  $\mu$ g/12 h) mice. All tumors of each group were collected, weighed and examined at the end of either the second, third or fourth week of treatment (Fig. 3e,f). In all treated mice, EBV-induced tumor growth either ceased or was inhibited (Fig. 3e,f). In contrast, all EBV-free tumors, as well as all tumors of controls, continued growing until the end of the experiments (Fig. 3e,f). Figure 3e,f and Table 1 show the differences in sizes and weights of the EBV-induced tumors in treated mice compared with other tumors in treated and control mice. Microscopic examination showed that mass proliferation existed in EBV-free lymphomas of treated mice, as well as all tumors of controls (Fig. 3g), whereas massive coagulative necrosis spread to all EBV-induced tumors in treated mice (Fig. 3h). There were significant differences in the sums of the tumor weights between control and treated EBV-induced lymphomas (SCID mice) ( $P < 0.05$ , rank-order analysis, Mann-Whitney test) (Table 1).

In BALB/c nude mice, non-small cell or small cell lung cancer cells were inoculated at the left armpit and a 14-d treatment involving three daily intraperitoneal injections was started 4 d after inoculation. At the end of the experimental period, tumors of control mice ( $n = 5$ , intraperitoneal control solution 0.3 ml/8 h) continued to grow (Fig. 3i,j), whereas the growth of tumors in treated mice ( $n = 5$ , intraperitoneal PMC-LC 350  $\mu$ g/8 h) was reduced. Microscopic examination revealed extensive necrosis of cancerous cells in treated tumors (Supplementary Fig. 4 online).

**Table 1 Median, maximum and minimum weights of implanted tumors**

Strains	Tumor	Treatment	Number	Growth time (d)	Weight (mg)		
					Median	Min.	Max.
SCID beige	EBV <sup>-</sup> BL	Control	5	16 <sup>a</sup>	182	98	283
			5	23	360	105	511
			5	32	546	532	644
		PMC-EBV-treated	5	16 <sup>a</sup>	200	182	293
			5	23	235	208	434
			5	32	563	279	614
	EBV <sup>+</sup> BL	Control	5	16 <sup>a</sup>	102	63	110
			5	23	180	122	687
			5	32	460	203	1,069
		PMC-EBV-treated	5	16 <sup>a</sup>	32	14	44
			5	23	179	43	405
			5	32	203	12	357
BALB/c	EBV <sup>+</sup> BL	Control	10	28 <sup>b</sup>	845	295	1,132
		PMC-EBV-treated	10		67	0	121
	Non LC	Control	5	18 <sup>c</sup>	236	119	544
		PMC-LC-treated	5		193	35	357
	Small LC	Control	5	18 <sup>c</sup>	374	211	1,165
		PMC-LC-treated	5		371	154	518

<sup>a</sup>The PMC-EBV treatment started at 2 d after tumor inoculation and lasted 14, 21 and 30 d respectively. <sup>b</sup>The PMC-EBV treatment started at 8 d after tumor inoculation and lasted 20 d. BL, Burkitt's lymphoma. <sup>c</sup>The PMC-LC treatment started at 4 d after tumor inoculation and lasted 14 d. Non LC, Non-small cell lung cancer; Small LC, Small cell lung cancer.

### *In vivo* targeting and accumulation of mimetics and fusions

*In vivo* distributions of the synthetic V<sub>H</sub>CDR1-V<sub>H</sub>FR2-V<sub>L</sub>CDR3 mimetic, HB-168 IgG, PMC-EBV, HB-8627 IgM and PMC-LC molecules were observed in BALB/c and SCID mice each bearing the following tumor-types (Fig. 4): (i) both 2- to 3-week-old EBV-induced and EBV-free Burkitt's lymphomas, (ii) EBV-induced Burkitt's lymphoma and non-small cell lung cancer, (iii) non-small cell lung cancer alone or (iv) 5-week-old EBV-induced Burkitt's lymphoma alone<sup>27,28</sup>. *In vivo* fluorescein isothiocyanate (FITC)-labeling of BALB/c mice revealed that PMC-EBV molecules penetrated into

EBV-induced tumors within 1 h after intraperitoneal injection (200 µg/mouse) and then gradually accumulated in the tumor cores. Such accumulation spread to the whole tumor area within 3 h after injection, but no similar accumulation was observed in EBV-free tumors. 6 h after injection, about 20% of accumulated PMC-EBV molecules still remained in the tumors, whereas >90% of the labels had been cleared from other areas and the abdominal cavity (Fig. 4b). In contrast, there was hardly any accumulation of parent HB-168 IgG (400 µg/mouse) in the cores of EBV-induced tumors, except slight accumulation along their boundaries (Fig. 4c). No PMC-SA molecules (200 µg/mouse; control) accumulated in either tumor (Fig. 4d). In BALB/c mice each bearing a 5-week-old, EBV-induced Burkitt's lymphoma alone, after 3 h, the accumulation of PMC-EBV molecules spread to the whole core area of lymphoma (tumors were incised to show accumulation in the core area) (Fig. 4e). There was no PMC-LC accumulation in 5-week-old lymphoma (Fig. 4g). Again, the FITC patch on the upper-left surface and less accumulation in the core area of the tumor demonstrated the inferior capacity of the parent antibody to penetrate tumors (Fig. 4f).

In BALB/c mice each bearing a 2-week-old non-small cell lung cancer alone (tumors were incised to show accumulation in the core area), the PMC-LC molecules displayed similar accumulation as the PMC-EBV selectively accumulated in mice bearing Burkitt's lymphoma (Fig. 4h). Although HB-8627, the parent antibody of PMC-LC, apparently displayed better accumulation in the tumor core than HB-168, the extent of penetration was still less than that of PMC-LC (Fig. 4i). In BALB/c mice bearing both 3-week-old EBV-induced Burkitt's lymphoma and 2-week-old non-small cell lung cancer, PMC-LC molecules accumulated only in the cores of non-small cell lung cancer tumors (Fig. 4j).

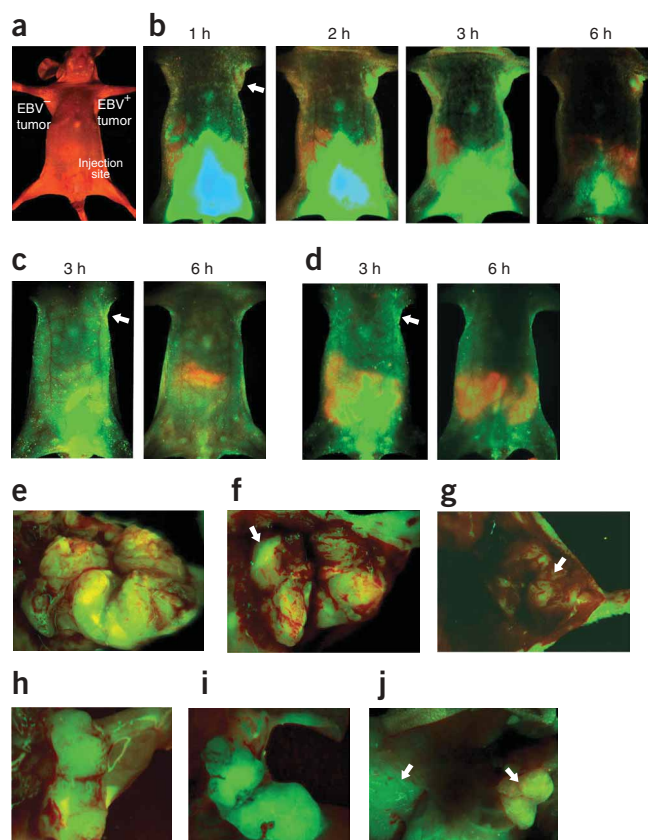


**Figure 4** Fluorescence images of tumors in BALB/c mice treated with FITC-labeled PMC-EBV, HB-168 IgG, PMC-SA, PMC-LC or HB-8627 IgM. Green fluorescence signals marked the location of FITC-labeled molecules. (a) The location of 2-week-old EBV-induced (EBV<sup>+</sup>) and EBV-free (EBV<sup>-</sup>) Burkitt's lymphomas. (b) Images of PMC-EBV showed that within 1 h after intraperitoneal injection, PMC-EBV molecules penetrated into the EBV-induced tumor (arrow) then gradually accumulated in the core area of the tumor. (c,d) Conversely, images of HB-168 IgG (c) and PMC-SA (d) showed that no essential agent molecules accumulated in any tumors, except where a small amount of HB-168 IgG accumulated along the boundaries of the EBV-induced tumor (arrow). (e-j) Tumors were incised to show possible accumulation of agents in their cores. PMC-EBV accumulated in the core area (e), whereas HB-168 IgG had mass accumulation at the surface (arrow) but less accumulation in the core area of 5-week-old Burkitt's lymphoma (f) and PMC-LC failed to show any accumulation (arrow) (g). (h,i) PMC-LC accumulated in the core area of incised 2-week-old non-small lung cancer (h), whereas HB-8627 IgM had less accumulation in the core area (i). (j) In BALB/c mice each bearing both EBV-induced lymphoma (BL, left arrow) and non-small cell lung cancer (LC, right arrow), PMC-LC selectively accumulated in the core area of lung cancer only.

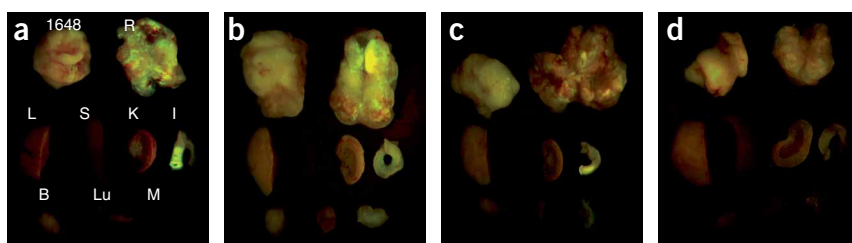


**Figure 5** Fluorescence images of tumors in SCID mice treated with FITC-labeled synthetic  $V_H$ CDR1- $V_H$ FR2- $V_L$ CDR3 mimetic, PMC-EBV or parent HB-168 IgG. Sectioned tumors and organs of SCID mice showed that synthetic  $V_H$ CDR1- $V_H$ FR2- $V_L$ CDR3 mimetics (a), as well as PMC-EBV molecules (b), selectively accumulated in the EBV-induced tumors. Conversely, the parent HB-168 IgG molecules were unable to reach the cores of tumors (c). (d) Mice treated with 0.9% saline solution served as controls. 1648, EBV-free tumor; R, EBV-induced tumor; L, liver; S, spleen; K, kidney; I, intestine; B, brain; Lu, lung; M, muscle.

Cross-sectioned tumors and organs of SCID mice, collected 3 h after fluorescent agents were injected intraperitoneally, revealed that the synthetic  $V_H$ CDR1- $V_H$ FR2- $V_L$ CDR3 mimetic, as well as PMC-EBV molecules, selectively accumulated in the cores of EBV-induced tumors (Fig. 5). Almost no parent HB-168 IgG molecules appeared in the cores of these tumors. The failure of the synthetic  $V_H$ CDR1- $V_H$ FR2- $V_L$ CDR3 mimetic and respective fusion molecules to accumulate in antigen-free tumors and host vital organs further confirms the targeting specificity of constructed  $V_H$ CDR1- $V_H$ FR2- $V_L$ CDR3 mimetics. Collectively, our data strongly suggest that the targeting specificity of the mimetics has driven their selective accumulation in the cores of solid tumors after intraperitoneal injection.

#### Assessment of toxicity of $V_H$ CDR1- $V_H$ FR2- $V_L$ CDR3 fusions

The immunocompromised mice bearing tumors that received the 14–20 d treatment with PMC-EBV remained healthy and gained bodyweight ( $n = 60$ , intraperitoneal PMC-EBV 350  $\mu$ g/mouse/each day; Supplementary Fig. 5 online). Normal mice that received the same treatment with doubled dosages over 30 d ( $n = 20$ , intraperitoneal PMC-EBV 700  $\mu$ g/mouse/each day; Supplementary Fig. 5 online) also gained body weight and there was no microscopic evidence of necrosis, inflammation or lymphocyte infiltration in the livers, intestines, kidneys or spleens. Indirect enzyme-linked immunosorbent assay (ELISA) assay found no detectable antibodies against respective epitopes in normal mice after the 2-week treatment with either synthetic  $V_H$ CDR1- $V_H$ FR2- $V_L$ CDR3 mimetic ( $n = 5$ ), wild-type colicin Ia ( $n = 5$ ) or PMC-EBV ( $n = 5$ ) by daily intraperitoneal injection. Although the data suggest that toxin-mimetic fusion peptides may be tolerated by mammals without evident toxicity or immunogenicity, the potential immunogenicity associated with systemic use in humans needs to be investigated.

#### DISCUSSION

In pursuing our initial goal to create single-chain, high-affinity antibody mimetics that target and penetrate solid tumors, we first aimed to identify whether such single-chain entities retained the recognition abilities of the parent antibodies and then examined whether they might be used to construct fusion molecules for diagnostic or therapeutic applications associated with cancer.

The antigen-binding capacities of our single-chain mimetics suggest that appropriate orientation of the  $V_H$  and  $V_L$  domains, conferred by an FR spacer probably ensures retention of partial synergic interactions of the  $V_H$  and  $V_L$  domains.

To determine the optimal pair of  $V_H$  and  $V_L$  domain CDRs with the best retained synergic interactions, we constructed four mimetics based on HB-168, a monoclonal IgG against the EBV envelope glycoprotein gp350/220. We made four mimetics, each composed of two CDRs, either CDR1 or CDR2 of a variable domain, recombined with CDR3 of the other variable domain. The two CDRs were connected with a selected FR2. Among all constructed mimetics,  $V_H$ CDR1- $V_H$ FR2- $V_L$ CDR3 retained the highest antigen-recognition ability, as measured by competitive inhibition of the parent antibody activity (Fig. 1d,e). The results of *in vivo* distribution and targeted tumor growth inhibition indicated that, relative to

the parent antibody, the synthetic  $V_H$ CDR1- $V_H$ FR2- $V_L$ CDR3 mimetic and toxin-mimetic fusions both had enhanced capacity to penetrate and accumulate in solid tumors (Figs. 4 and 5). The apparent disadvantage of mimetics without a framework linkage, for example, the  $V_H$ CDR1- $V_L$ CDR3 mimetic and a ‘cyclic’ peptide containing key residues of all six CDRs<sup>8,9</sup>, is the lack of a ‘quasi-physiological’ linkage (Supplementary Fig. 6 online) between the CDR derivatives to support their interaction with antigenic epitopes through an appropriate interface.

Our findings suggest that with the linkage of the selected framework region in  $V_H$ CDR1- $V_H$ FR2- $V_L$ CDR3 mimetics, the structural orientation of the two CDRs probably approximates that of their native counterparts in the antibody-antigen complex, ensuring retention of their antigen-recognition activities. Moreover, with the synergic interaction of the CDR1 loop of the other variable domain, the selected CDR3 loop of the mimetic might be extended far beyond the ‘flat’ surface of the parent antibody to enhance targeting activity<sup>5</sup>. Similar to systems predating the evolution of immunoglobulins, the mimetic might access antigenic epitopes with merely two CDRs through the ‘quasi-physiological’ linkage of the connecting framework region (Supplementary Fig. 6 online). Our competition studies to assess inhibition of parent antibody binding by mimetics indicated that mimetics without any framework region joining the selected CDRs retained hardly any activity. In contrast, the mimetic composed of the same CDRs, but connected with a FR, could compete with the parent antibody for antigen binding (Fig. 1e). Among all framework regions of the parent antibody, the selected framework region  $V_H$ FR2 contains the fewest hydrophobic patches. This structural advantage presumably reduces the risk of aggregation, as demonstrated by PAGE, sizing chromatography and artificial lipid bilayer assays (Supplementary Fig. 2 online).

One goal of recombining antibodies, Fab fragments and mimetics is to design ‘continuous-sequence’ mimetics of discontinuous native CDRs for enhanced affinity in simplified structures<sup>5,9,10</sup>. In a striking example, a point mutation increased hapten-binding affinity of an scFv fragment 1,800-fold<sup>29</sup>. Blindly increased affinity, however, might approach an upper limit of antigen-binding affinity beyond which further increases in affinity do not enhance tumor localization<sup>30</sup>. Previous studies found that the lowest-affinity scFv had the most uniform distribution throughout the tumor, whereas the highest-affinity scFv was found mainly in the perivascular region of the tumor<sup>31</sup>. To avoid such a ‘binding-site barrier’, we have retained weakened affinity instead of enhanced affinity of parent antibody against targets through recombination of the minimum number of  $V_H$

and  $V_L$  CDR units in a single-chain mimetic. As an empirical approach, the results of binding/competitive inhibition assays indicated that the retained binding affinity of the  $V_H$ CDR1- $V_H$ FR2- $V_L$ CDR3 mimetic was only ~1–10% of the value of binding affinity of the parent antibody (Fig. 2b,c). With such reduced affinity, PMC-EBV molecules had enhanced recognition ability against cells bearing a high-density of surface antigens, but did not behave substantially differently from the parent antibody in recognizing cells that carry potential cross-reacting antigens on their surface (Fig. 2d).

*In vivo* imaging indicated that the synthetic mimetic and related fusion peptides both presented enhanced tumor localization and penetration ability as postulated previously<sup>32</sup> (Figs. 4 and 5). An abundance of specific antigens on the surfaces of many kinds of tumor cells was associated with fewer cross-reacting antigens binding to the surfaces of certain normal cells<sup>16,33</sup>. This suggests that  $V_H$ CDR1- $V_H$ FR2- $V_L$ CDR3 mimetics retaining weakened parent antibody affinity may recognize targeted tumor cells with sufficient numbers of surface antigens, but ignore cells with fewer cross-reacting antigenic epitopes. More precise measurements of the affinities of mimetics and comparison between mimetics and parental antibodies are needed to understand the physiological significance of redesigned binding pockets in mimetics.

The 70 kDa channel-forming bacteriocin colicin Ia has several advantages as an ideal toxic moiety of toxin-mimetic fusion molecules: it is a soluble and heat-stable monomeric exotoxin with relatively stable cytotoxicity and lacks cysteine residues that might potentially form disulfide bonds, causing aggregation<sup>20,21,23</sup>. There was neither poor solubility nor aggregation of fusions in either of the free or FITC-labeled forms (Supplementary Fig. 2 online). Additionally, toxicity assessment in normal mice (Supplementary Fig. 5 online) and indirect ELISA assays suggest that colicin may not be immunogenic. Compared with other toxic moieties ranging from 50 to 70 kDa, such as *Pseudomonas aeruginosa* exotoxin, *Corynebacterium diphtheria* toxin and angiogenin<sup>34–36</sup>, our results indicate that colicin Ia has very effective killing activity and behaves as an ideal indicator to evaluate the antigen-recognition ability of constructed mimetics *in vitro* and *in vivo*. However, the smaller molecular weight toxin-mimetic fusion peptides may hold more promise against solid tumors with less risk of immunogenicity.

A common functional feature among four constructed  $V_H$ CDR1- $V_H$ FR2- $V_L$ CDR3 mimetics, derived from cognate CDRs and framework region sequences of various antibodies or scFv, is the retention of the specificity and reduced affinity of parent antibody against related antigens. Tumor xenograft studies indicate that two pheromonicins, PMC-EBV and PMC-LC, possess superior tumor penetration activities than their parent antibodies and effectively inhibit tumor growth *in vivo*. Taken together, our results suggest that a variety of specific antibodies can be tailored to construct mimetics comprising two CDRs, each selected from the  $V_H$  and  $V_L$  domain of a Fab, oriented by means of a framework region. Such mimetics may hold promise for markedly improving cancer diagnostics and therapeutics, especially as the small size of the mimetic may confer other useful properties, such as enhanced intracellular delivery.

## METHODS

**Preparation of mimetics and fusion molecules.** DNA sequences of  $V_H$  and  $V_L$  domains of antibody and scFv against lymphocyte differentiation antigens CD8 and CD23 were published previously (NCBI accession numbers AAB58061, AAB58062, CAC07533 and CAC07534, respectively).  $V_H$  and  $V_L$  domain genes for monoclonal IgG against EBV gp350/220 envelope glycoprotein and monoclonal IgM against non-small cell lung cancer surface antigen were obtained

from DNA isolated from ATCC HB-168 and HB-8627 mouse hybridoma cells, respectively<sup>15–19</sup>. ATCC HB-168 and HB-8627 murine hybridoma cell lines were grown in RPMI 1640 with 10% FBS to a density of  $10^7$  cells/ml. Total RNA was extracted and amplified by RT-PCR (Takara RNA PCR Kit (AMV Ver.3.0)), purified RT-PCR products were ligated into the plasmids pMD18-T, which were purchased from Takara. The DNAs of plasmids were isolated and analyzed to determine the genes of  $V_H$  and  $V_L$  domains of monoclonal antibodies. Harvested monoclonal antibodies (mAbs) were stored at  $-20^\circ\text{C}$  for subsequent experiments. For example, the genes of  $V_H$ CDR1,  $V_H$ FR2 and  $V_L$ CDR3 regions of mAbs or scFv were constructed to follow position 1626 of colicin Ia by double-stranded oligonucleotide mutagenesis (QuickChange kit, Stratagene) using a plasmid containing the colicin Ia gene to form pheromonicin-EBV (PMC-EBV)<sup>24</sup>. The oligonucleotides used contained the desired mutations; for example, for SFGMHVWRQAPEKGLEWVAGQGYSYPYT of HB-168 mAb, the oligos were 5'-GCG AAT AAG TTC TGG GGT ATT TCC TTC GGT ATG CAT TGG GTG CGT CAG TAA ATA AAA TAT AAG ACA GGC-3', 5'-GGT ATG CAT TGG GTG CGT CAG GCC CCC GAG AAA GGT CTG GAG TGG GTG GCC TAA ATA AAA TAT AAG ACA GGC -3' and 5'-AAA GGT CTG GAG TGG GTG CGT GCC GGT CAG GGT TAC TCC TAC CCC TAC ACC TAA ATA AAA TAT AAG ACA GGC -3' (boldface triplets represent inserted mimetic genes). PMC-EBV was expressed and purified as described previously<sup>24,26,37</sup>. The total protein concentration of elute was about 1 mg/ml. The purified proteins were placed in the 20 mM phosphate buffer, pH 7.4, with 0.2 M NaCl and 2 mM EDTA by dialysis from borate buffer. Sizing chromatography was performed with 2410 refractive index detector/2487 Dual-lambda absorbance detective/2690 Separations module (Walters Co.) with TSK-gel G3000SW column. Channel-forming experiments were done on planar lipid bilayer membranes formed at  $20$ – $22^\circ\text{C}$  from asolectin (Lecithin type IIS; Sigma)<sup>21,37</sup>.

**Amino acid sequences of mimetics.** The sequence of the 'cyclic' mimetic containing 'active' polar and hydrophobic residues of all six CDRs in an HB-168 IgG Fab is CAWPHYDYPPHYADVKGPYSYPKNPYGPRM. The sequences of the  $V_H$ CDR1- $V_H$ FR2- $V_L$ CDR3 mimetics of the following parent molecules are:

HB-168 IgG: SFGMHVWRQAPEKGLEWVAGQGYSYPYT  
 HB-8627 IgM: DYLLHWVKRTEQGLEWIGQHIRELTRS  
 IgG against CD8 : DYNMHWVKQSHGKSLEWIGQQNEDPPT  
 scFv against CD23: GYWMSVWRQAPGKGLEWVAQQLVEYPPFT.

***In vitro* killing activity and immunolabeling assays.** The cell lines of Burkitt's lymphoma (ATCC CCL-86), AIDS-related body cavity-based lymphoma (ATCC CRL-2230), nasopharyngeal cancer (HNE1, Hunan Univ. Med. Sci.), EBV-free Burkitt's lymphoma (ATCC CRL-1648), EBV-free nasopharyngeal cancer (HNE3, Hunan Univ. Med. Sci.), non-small cell lung cancer (ATCC CCL-185), small cell lung cancer (SP-CA-1, Peking Union Med. Coll.), acute T-cell leukemia (ATCC TIB-152), human hepatocellular carcinoma (SMMC-7721, Peking Union Med. Coll.), human umbilical venous endothelium (ATCC ECV-304) and mouse fibroblast (ATCC 3T3) were inoculated in Falcon 3046 six-well tissue culture plates (Becton Dickinson Co.) with 3 ml of 1640 medium at an initial cell density of  $5 \times 10^5$  cell/ml and grown at  $37^\circ\text{C}$  in  $\text{CO}_2$  incubator (Sanyo Electro. Biomed.). CCL-86 Burkitt's lymphoma (BL) cells were grown in 5 ml 1640 medium for 72 h, fixed in 4% paraformaldehyde then incubated with 10% BSA/PBS, incubated with corresponding 100  $\mu\text{l}$  synthetic mimetics (0.25 mg/ml),  $V_H$ CDR1- $V_H$ FR2- $V_L$ CDR3,  $V_H$ CDR2- $V_H$ FR2- $V_L$ CDR3,  $V_L$ CDR1- $V_L$ FR2- $V_H$ CDR3,  $V_L$ CDR2- $V_L$ FR2- $V_H$ CDR3,  $V_H$ CDR3- $V_H$ FR2- $V_L$ CDR3 or  $V_H$ CDR1- $V_H$ FR2- $V_H$ CDR3 (CL (Xian) Bio-Scientific) or 10 mM PBS and murine HB-168 IgG (1 mg/ml), incubated with FITC-labeled secondary rabbit anti-mouse antibody (1 mg/ml, DAKO A/S), suspended with 100  $\mu\text{l}$  of 10 mM PBS containing DAPI fluorescent dye (30 ng/ml), dripped on the slide and observed under an inverted fluorescent microscope (Nikon TE2000u) at  $400\times$  with UV-2E/C and B-2E/C filters. Different concentrations ranging from 5 to 125  $\mu\text{g}/\text{ml}$  were used for the PMC-EBV and controls: wild-type colicin Ia and PMC-SA<sup>24</sup>. Cultured BL cells were suspended with 100  $\mu\text{l}$  of 1640 medium after centrifugation. Then living and dead cells were counted with 0.2% Trypan blue and 50 nM acridinorange/600 nM propidium iodide double-staining. Vital staining data were collected with digital data collection under an inverted fluorescent microscope (IX-71, Olympus) at  $400\times$  with U-MWU2,

U-MNB2 and U-MNG2 filters. Harvested HB-168 monoclonal IgG and synthetic V<sub>H</sub>CDR1-V<sub>H</sub>FR2-V<sub>L</sub>CDR3 mimetic were used for concentration-dependent inhibitory experiments against the killing activity of PMC-EBV. Different concentrations of either HB-168 mAb, or synthetic V<sub>H</sub>CDR1-V<sub>H</sub>FR2-V<sub>L</sub>CDR3 of HB-168 mAb were added with PMC-EBV (50 µg/ml) to incubate with BL cells, then cells were treated and observed as described above<sup>38</sup>. CCL-86 or CRL-1648 Burkitt's lymphoma (BL) cells were grown in 5 ml 1640 medium for 72 h, fixed in 4% paraformaldehyde then 100 µl fixed cells (10<sup>4-7</sup>/ml) were incubated with 10 µl synthetic mimetics, V<sub>H</sub>CDR1-V<sub>H</sub>FR2-V<sub>L</sub>CDR3, V<sub>H</sub>CDR3-V<sub>H</sub>FR2-V<sub>L</sub>CDR3 or V<sub>H</sub>CDR2-V<sub>H</sub>FR2-V<sub>L</sub>CDR3 (CL (Xian) Bio-Scientific) and V<sub>H</sub>CDR1-V<sub>L</sub>CDR3, V<sub>H</sub>CDR1-V<sub>H</sub>CDR3 or V<sub>H</sub>CDR3-V<sub>L</sub>CDR3 (South West University), or HB-168 IgG with different concentrations (10<sup>3</sup> to 10<sup>-1</sup> nM) for 50 min at 37 °C, then incubated with 10 µl PMC-EBV (1 mg/ml) or HB-168 IgG (2 mg/ml) for 50 min at 37 °C. Mean fluorescent intensity of per 2,000 cells was measured by BD FACSCanto Flow Cytometer (BD Biosciences).

**In vivo tumor models.** Human Burkitt's lymphoma (EBV-free, ATCC CRL-1648 and EBV-induced, ATCC CCL-86), non-small cell lung cancer (ATCC CCL-185) and small cell lung cancer (SP-CA-1) cells were used for implantation into immunodeficiency SCID Beige and BALB/c athymic nude mice. Four- to 5-week-old SCID mice and BALB/c mice, weighing 16–20 g were prepared and cared for by the Experimental Animal Center, Sichuan University. Each SCID mouse was inoculated with EBV-induced (left side) and EBV-free (right side) BL cells at the corresponding armpit through subcutaneous injection with about 0.2–0.3 ml (3–5 × 10<sup>8</sup> cells/ml) tumor cells. BALB/c mice were inoculated with EBV-induced BL or non-small cell lung cancer or small lung cancer cells at left armpit only through the same injection and cell amount. Tumor growth was monitored daily until it reached the acceptable sizes. The mice were injected intraperitoneally with PMC-EBV at 350 µg/mouse/day or PMC-LC at 1,050 µg/mouse/day for 14–20 d. SCID mice were injected intraperitoneally with PMC-EBV at 700 µg/mouse/day for 30 d. For *in vivo* fluorescent imaging, mice were inoculated with BL or non-small cell lung cancer cells alone or both BL and non-small cell lung cancer cells without treatment. Mice were killed at the end of experiments and the entire armpit area and visceral organs were collected for tumor quantification and histopathology examination. The total weight of each group of tumors was analyzed with *t*-test and Mann-Whitney test with SPSS software. Tissues were either fixed in 4% paraformaldehyde, dehydrated in graded alcohols, embedded in paraffin or frozen at -25 °C for sectioning. Sections were stained with hematoxylin and eosin. Kunming normal mice, weighing 16–20 g were injected with either synthetic V<sub>H</sub>CDR1-V<sub>H</sub>FR2-V<sub>L</sub>CDR3 mimetic (*n* = 5), or wild-type colicin Ia (*n* = 5) or PMC-EBV (*n* = 5) intraperitoneally each day. After 2 to 3 weeks of treatment, mice were killed for histopathological inspection or blood samples were collected for indirect ELISA to screen potential antibodies.

**In vivo fluorescence imaging.** BALB/c and SCID mice, each weighing 16–20 g, were inoculated with EBV-induced (left) and EBV-free (right) BL cells, or non-small cell lung cancer (left) and EBV-induced (right) tumor cells at armpits. Synthetic V<sub>H</sub>CDR1-V<sub>H</sub>FR2-V<sub>L</sub>CDR3 mimetic of HB-168 IgG, PMC-EBV, PMC-LC, PMC-SA, HB-168 IgG or HB-8627 IgM were labeled with FITC (EZ-labeled FITC protein labeling kit, Pierce Biotech). For BALB/c mice, 200 µg FITC-labeled pheromonicins (*n* = 5) or mAbs (*n* = 5) were injected intraperitoneally 2 to 5 weeks after tumor cells were inoculated. The mice were placed under anesthesia by ether inhalation and fastened on a board. For SCID mice, FITC-labeled synthetic V<sub>H</sub>CDR1-V<sub>H</sub>FR2-V<sub>L</sub>CDR3 mimetic of HB-168 IgG (*n* = 5), PMC-EBV (*n* = 5), HB-168 IgG (*n* = 5) or 0.9% saline (*n* = 5) was injected intraperitoneally 20–22 d after tumor cells were inoculated. Mice were killed 3 h after injection, then tumors and vital organs were sectioned. The images were observed every hour after injection with the LT-99D2 Illumatoool Dual Light System (excitation 470 nm, emission 515 nm, Lighttools Research) and recorded by a built-in CCD camera. The fluorescence brightness at tumor and abdominal areas was measured with Image-pro plus 4.5 software (Media-Cybernetics). All *in vivo* protocols were approved by the Institutional Animal Care and Use Committee of Sichuan University and Project of Sichuan Animal Experiment Committee, license 045, China.

Note: Supplementary information is available on the Nature Biotechnology website.

## ACKNOWLEDGMENTS

This work was supported by National Science Foundation of China grants 30430220, 30271557, 30571942 and 30672137 and Program for Changjiang Scholars and Innovative Research Team in University, Ministry of Education to X.-Q.Q. and H.W. We would like to acknowledge the help and scientific critique of P. Kienker, H. Li, J.C. Hou and C.A. Deng during the preparation of this manuscript. We would also like to acknowledge the help of J. Zhang, P. Dai, Z.P. Zhen, Y.C. Huang, F.L. Cai, S.Y. Qiu and X.F. Lu in DNA scanning, histology and fusion peptide purification.

## AUTHOR CONTRIBUTIONS

X.-Q.Q. and H.W. prepared mimetics and fusion molecules, measured *in vitro* and *in vivo* killing activity and did immunolabeling/fluorescent/pathology assays; B.C. and L.-L.W. did the cytometry assays; S.-T.Y. carried out SDS-PAGE and sizing chromatography.

## COMPETING INTERESTS STATEMENT

The authors declare no competing financial interests.

Published online at <http://www.nature.com/naturebiotechnology>

Reprints and permissions information is available online at <http://npg.nature.com/reprintsandpermissions>

1. Hoogenboom, H.R. Selecting and screening recombinant antibody libraries. *Nat. Biotechnol.* **23**, 1105–1116 (2005).
2. Borg, N.A. *et al.* The CDR3 regions of an immunodominant T cell receptor dictate the 'energetic landscape' of peptide-MHC recognition. *Nat. Immunol.* **6**, 171–180 (2005).
3. Laune, D. *et al.* Systematic exploration of the antigen binding activity of synthetic peptides isolated from the variable regions of immunoglobulins. *J. Biol. Chem.* **272**, 30937–30944 (1997).
4. Ewert, S., Huber, T., Honegger, A. & Plückthun, A. Biophysical properties of human antibody variable domains. *J. Mol. Biol.* **325**, 531–553 (2003).
5. Holliger, P. & Hudson, P. Engineered antibody fragments and the rise of single domains. *Nat. Biotechnol.* **23**, 1126–1136 (2005).
6. Binz, H.K., Amstutz, P. & Plückthun, A. Engineering novel binding proteins from nonimmunoglobulin domains. *Nat. Biotechnol.* **23**, 1257–1267 (2005).
7. Binz, H.K. *et al.* Engineered proteins as specific binding reagents. *Curr. Opin. Biotechnol.* **16**, 459–469 (2005).
8. Heap, C.J. *et al.* Analysis of a 17-amino acid residue, virus-neutralizing microantibody. *J. Gen. Virol.* **86**, 1791–1800 (2005).
9. Casset, F. *et al.* A peptide mimetic of an anti-CD4 monoclonal antibody by rational design. *Biochem. Biophys. Res. Commun.* **307**, 198–205 (2003).
10. Qin, W. *et al.* Fusion protein of CDR mimetic peptide with Fc inhibit TNF- $\alpha$  induced cytotoxicity. *Mol. Immunol.* **43**, 660–666 (2006).
11. Souriau, C. *et al.* New binding specificities derived from Min-23, a small cysteine-stabilized peptide scaffold. *Biochemistry* **44**, 7143–7155 (2005).
12. Aburatani, T., Ueda, H. & Nagamune, T. Importance of a CDR H3 basal residue in V<sub>H</sub>/V<sub>L</sub> interaction of human antibodies. *J. Biochem.* **132**, 775–785 (2002).
13. De Genst, E. *et al.* Chemical basis for the affinity maturation of a camel single domain antibody. *J. Biol. Chem.* **279**, 53593–53601 (2004).
14. Rothlisberger, D., Honegger, A. & Plückthun, A. Domain interactions in the Fab fragment: a comparative evaluation of the single-chain Fv and Fab format engineered with variable domains of different stability. *J. Mol. Biol.* **347**, 773–789 (2005).
15. Hoffman, G.J. *et al.* Monoclonal antibody against a 250,000-dalton glycoprotein of Epstein-Barr virus identifies a membrane antigen and a neutralizing antigen. *Proc. Natl. Acad. Sci. USA* **77**, 2979–2983 (1980).
16. Hellstrom, I. *et al.* Monoclonal mouse antibodies raised against human lung carcinoma. *Cancer Res.* **46**, 3917–3923 (1986).
17. Gong, M. & Kieff, E. Intracellular trafficking of two major Epstein-Barr virus glycoproteins, gp350/220 and gp110. *J. Virol.* **64**, 1507–1516 (1990).
18. Thorley-Lawson, D.A. & Gross, A. Persistence of the Epstein-Barr virus and the origins of associated lymphomas. *N. Engl. J. Med.* **350**, 1328–1337 (2004).
19. Thorley-Lawson, D.A. & Geilinger, K. Monoclonal antibodies against the major glycoprotein (gp350/220) of Epstein-Barr virus neutralize infectivity. *Proc. Natl. Acad. Sci. USA* **77**, 5307–5311 (1980).
20. Cramer, W.A. *et al.* Structure-function of the channel-forming colicins. *Annu. Rev. Biophys. Biomol. Struct.* **24**, 611–641 (1995).
21. Qiu, X.-Q., Jakes, K.S., Kienker, P.K., Finkelstein, A. & Slatin, S.L. Major transmembrane movement associated with colicin Ia channel gating. *J. Gen. Physiol.* **107**, 313–328 (1996).
22. Kienker, P.K., Qiu, X.-Q., Slatin, S.L., Finkelstein, A. & Jakes, K.S. Transmembrane insertion of the colicin Ia hydrophobic hairpin. *J. Membr. Biol.* **157**, 27–37 (1997).
23. Jakes, K.S., Kienker, P.K. & Finkelstein, A. Channel-forming colicins: translocation (and other deviant behaviour) associated with colicin Ia channel gating. *Q. Rev. Biophys.* **32**, 189–205 (1999).

24. Qiu, X.Q. *et al.* An engineered multidomain bactericidal peptide as a model for targeted antibiotics against specific bacteria. *Nat. Biotechnol.* **21**, 1480–1485 (2003).
25. Qiu, X.Q., Zhang, J., Wang, H. & Wu, G.Y. A novel engineered peptide, a narrow-spectrum antibiotic, is effective against vancomycin-resistant *Enterococcus faecalis*. *Antimicrob. Agents Chemother.* **49**, 1184–1189 (2005).
26. Jakes, K.S., Abrams, C.K., Finkelstein, A. & Slatin, S.L. Alteration of the pH-dependent ion selectivity of the colicin E1 channel by site-directed mutagenesis. *J. Biol. Chem.* **265**, 6984–6991 (1990).
27. Gao, X. *et al.* *In vivo* cancer targeting and imaging with semiconductor quantum dots. *Nat. Biotechnol.* **22**, 969–976 (2004).
28. Yu, Y.A. *et al.* Visualization of tumors and metastases in live animals with bacteria and vaccinia virus encoding light-emitting proteins. *Nat. Biotechnol.* **22**, 313–320 (2004).
29. Midelfort, K.S. *et al.* Substantial energetic improvement with minimal structural perturbation in a high affinity mutant antibody. *J. Mol. Biol.* **343**, 685–701 (2004).
30. Carter, P.J. Potent antibody therapeutics by design. *Nat. Rev. Immunol.* **6**, 343–357 (2006).
31. Adams, G.P. *et al.* High affinity restricts the localization and tumor penetration of single-chain Fv antibody molecules. *Cancer Res.* **61**, 4750–4755 (2001).
32. Fujimori, K., Covell, D.G., Fletcher, J.E. & Weinstein, J.N. Modeling analysis of the global and microscopic distribution of immunoglobulin G, F(ab')<sub>2</sub>, and Fab in tumors. *Cancer Res.* **49**, 5656–5663 (1989).
33. Mattes, M.J. *et al.* Cell surface antigens of human ovarian and endometrial carcinoma defined by mouse monoclonal antibodies. *Proc. Natl. Acad. Sci. USA* **81**, 568–572 (1984).
34. Bang, S., Nagata, S., Onda, M., Kreitman, R.J. & Pastan, I. HA22(R490A) is a recombinant immunotoxin with increased antitumor activity without an increase in animal toxicity. *Clin. Cancer Res.* **11**, 1545–1550 (2005).
35. Vallera, D.A. *et al.* Molecular modification of a recombinant, bivalent anti-human CD3 immunotoxin (Bic30) results in reduced *in vivo* toxicity in mice. *Leuk. Res.* **29**, 331–341 (2005).
36. Krauss, J. *et al.* Targeting malignant B-cell lymphoma with a humanized anti-CD22 scFv-angiogenin immunoenzyme. *Br. J. Haematol.* **128**, 602–609 (2005).
37. Qiu, X.Q., Jakes, K.S., Finkelstein, A. & Slatin, S.L. Site-specific biotinylation of colicin Ia: A probe for protein conformation in the membrane. *J. Biol. Chem.* **269**, 7483–7488 (1994).
38. Harlow, E. Lane, D. (eds.) *Immunohistochemistry. In Using Antibodies, A Laboratory Manual.* Chapter 6. Cold Spring Harbor Laboratory Press (1998) (Science Publication, Beijing, 93–129 (2002)).